INORGANIC CHEMISTRY FRONTIERS

RESEARCH ARTICLE

View Article Online
View Journal | View Issue

Cite this: *Inorg. Chem. Front.*, 2024, **11**, 7464

Excellent temperature sensitivities based on the FIR technique of up-conversion luminescence in a novel $NaLaTi_2O_6:Yb^{3+},Tm^{3+}$ material

Kai Li, [a,c] Zhiyu Zhang,[a] Daiman Zhu*[b] and Changtao Yue *[a]

Fluorescent luminescence thermometers possessing high temperature sensitivities have drawn extensive interest with increasing demand in daily life and industrial fields. However, thermal quenching usually takes place with increasing temperature for rare earth ion doped up-conversion luminescence phosphors. In this work, screened $NaLaTi_2O_6:Yb^{3+},Tm^{3+}$ materials were synthesized *via* a high-temperature solid-state reaction method. Strong blue and near-infrared up-conversion luminescence (UCL) emissions, as well as relatively weak red emissions, were observed under 980 nm laser excitation at room temperature. The emission bands of Tm^{3+} $^1G_4 \rightarrow {}^3H_6$ (blue), $^1G_4 \rightarrow {}^3F_4$ (red), and $^3H_4 \rightarrow {}^3H_6$ (near infrared) transitions significantly decayed with increasing temperature owing to the general thermal quenching effect. However, attractively, a negative thermal expansion effect, thermally boosted luminescence, appeared for Tm^{3+} $^3F_{2,3} \rightarrow {}^3H_6$ transition (deep red emission), which is likely to be derived from the phonon-assisted energy transfer effect. With the aid of high-contrast thermal-dependent characteristics of these transitions, extremely high maximal absolute and relative sensitivities of 4.29 K^{-1} at 653 K and 36.2% K^{-1} at 303 K, respectively, were achieved based on the proposed fluorescent intensity ratio (FIR) thermometry technique, which are one order of magnitude higher than previously reported results. These fascinating results indicate that the as-prepared materials could be excellent candidates for application in optical thermometry and encourage us to devise thermally boosted up-conversion and self-reference optical thermometers by utilizing Tm^{3+}-activated luminescence phosphors.

Received 2nd July 2024,
Accepted 2nd September 2024

DOI: 10.1039/d4qi01669f

rsc.li/frontiers-inorganic

1. Introduction

Non-contact and precise temperature monitoring is of growing significance in daily life, scientific research, medical diagnosis and treatment as well as industrial fields[1–3] However, conventional contact-type thermometers such as liquid-filled thermometers and thermocouples cannot meet the demands for modern society's development on account of their limited slow response speed and low sensitivity.[4] In contrast, non-contact optical thermometers, with the merits of remote detection, moving object temperature monitoring, swift response ability, high sensitivity, *etc.*, have gained considerable attention and currently have been a novel thermometer research hotspot.[5,6] Generally, optical thermometry is achieved by utilizing related temperature-dependent luminescence parameters of rare earth (RE) ion-activated phosphors. Herein, the phosphors, an essential component, can be integrated with a desired temperature detection device, and temperature detection is based on the phosphor's luminescence characteristics, including emission bandwidth, peak wavelength, fluorescent intensity, fluorescence decay lifetime (FL), and fluorescence intensity ratio (FIR).[7] Thus, the prospective application of phosphors with unique characteristics in non-contact thermometers is highly desired. Among the alternative techniques, FIR mode based on up-conversion luminescence (UCL) of rare earth ions has been widely studied.[8] Usually, this technique requires the distinct responses of two emissions with temperature, where one emission is taken as a reference signal and the other serves as an indicator signal. Previous works based on FIR mode mainly concentrate on thermally coupled energy levels (TCELs) as TCELs are easily found and utilized in rare earth ions such as Er^{3+} and Ho^{3+}.[9] However, the energy gap between two neighboring levels should be large enough to avert strong overlapping of these two emissions (>200 cm^{-1}) and small enough (<2000 cm^{-1}) to allow the lower level to have a minimum pumping of optically activated ions in the temperature range of interest. According to Boltzmann distribution,

[a]*College of Science, China University of Petroleum, Beijing, Beijing 102249, China. E-mail: yuect@cup.edu.cn*
[b]*Department of Energy Power and Mechanical Engineering, North China Electric Power University, Beijing, 102206, China. E-mail: zdm_uu@126.com*
[c]*Beijing Key Lab of Oil & Gas Optical Detection Technology, China University of Petroleum, Beijing, 102249, China*

generally, the larger energy gap intends to achieve a higher temperature sensitivity.[10] Consequently, further improvement of the temperature sensitivity is a large challenge owing to the restriction of the energy gap between the two TCELs.[11] Compared with the FIR technique based on the TCELs, the FIR technique based on the NTCELs by utilizing emitting energy levels from single or two luminescence centers is no longer limited by the energy separation, which may be likely to produce the higher sensitivity.[12,13] Thereby, utilizing two independent emissions based on non-thermally coupled energy levels (NTCEL) has become an important alternative mode for FIR thermometry to improve the detection sensitivity for temperature sensing.

Rare earth ions involving Er^{3+}, Ho^{3+}, Tm^{3+}, Nd^{3+} and so on have been extensively investigated as temperature detectors in phosphors.[14–16] However, the precision of optical thermometers may deviate ascribed to a lack of sufficient up-conversion emission intensity originating from their poor and narrow absorption cross-section in the near-infrared (NIR) region. Possessing the high absorption efficiency of the NIR region, Yb^{3+} is usually employed as the sensitizer in a phosphor to transfer the absorbed energy to activators, extremely enhancing the luminescence of activators.[17,18] However, The UCL thermal quenching effect of rare earth ions usually takes place in most hosts, which restricts the further improvement of the UCL temperature sensing technique. Tm^{3+} often produces blue, red and NIR emissions upon 980 nm excitation when sensitized by Yb^{3+}.[19] Moreover, Yb^{3+}, Tm^{3+} co-doped phosphors such as $NaGdTiO_4$:Yb^{3+},Tm^{3+}, $BaGd_2ZnO_5$:Yb^{3+}, Tm^{3+}, Sr_2LaNbO_6:Yb^{3+},Tm^{3+} have been reported to have good UCL and temperature sensing properties,[20–23] in which both TCEL ($^1G_{4(1)}$ and $^1G_{4(2)}$) and NTCEL ($^1G_4$ and $^3H_4$) levels from Tm^{3+} ions were adopted for optical thermometry calculation. Despite a large number of optical thermometers based on the Tm^{3+} FIR technique have been reported, utilizing negative thermal expansion effect (thermally boosted luminescence) from Tm^{3+} $^3F_{2,3} \rightarrow {}^3H_6$ transition and general thermal quenching transitions to design the high-performance FIR thermometry technique is rarely reported. As a consequence, exploring Yb^{3+}, Tm^{3+} co-doped phosphors possessing negative thermal expansion effect is of potential to realize the outstanding temperature sensing properties and stability based on the Tm^{3+} high-contrast temperature responses UCL of different emission bands.

In this work, a sequence of novel $NaLaTi_2O_6$:Yb^{3+},Tm^{3+} materials was screened and prepared. Using the energy transfer (ET) from Yb^{3+} to Tm^{3+}, the UCL of Tm^{3+} is highly enhanced when irradiated by a 980 nm laser. The temperature-dependent luminescence behavior of a representative $NaLa_{0.89}Ti_2O_6$:$0.10Yb^{3+}$,$0.01Tm^{3+}$ phosphor was studied in detail. Common thermal quenching of Tm^{3+} $^1G_4 \rightarrow {}^3H_6$, $^1G_4 \rightarrow {}^3F_4$, and $^3H_4 \rightarrow {}^3H_6$ transitions and a rare thermally boosted luminescence of Tm^{3+} $^3F_{2,3} \rightarrow {}^3H_6$ transition were found in this material. By utilizing the diverse temperature responses of these transitions, the temperature sensing property was investigated by monitoring the intensity ratio of these transitions at the temperature range from 303 to 653 K. Fascinatingly, the material presents ultra-high maximal absolute and relative sensitivities of 4.29 K^{-1}@653 K and 36.2% K^{-1}@303 K, respectively, which are one order of magnitude higher than the reported results. These results indicate that $NaLaTi_2O_6$:Yb^{3+},Tm^{3+} materials can be regarded as promising candidates for optical thermometry. Simultaneously, this work provides a new insight into devising novel optical thermometers with the aid of both thermal quenching and thermally boosted luminescence of Tm^{3+}-activated phosphors.

2. Experimental section

2.1 Samples preparation

A sequence of novel titanate materials with the chemical formula $NaLaTi_2O_6$ and $NaLa_{0.99-x}Ti_2O_6$:xYb^{3+},$0.01Tm^{3+}$ (x = 0, 0.05, 0.10, 0.20, 0.30) were prepared *via* a conventional high-temperature solid-state reaction method. Typically, raw materials involving Na_2CO_3 (A.R.), La_2O_3 (A.R.), TiO_2 (A.R.), Yb_2O_3 (99.9%) and Tm_2O_3 (99.9%), without further purification, were first stoichiometrically weighted and ground thoroughly in an agate mortar for about 15 min with a moderate dose of ethanol. Then, the mixture was transferred to corundum crucibles to calcine in a furnace for about 5 h at 1150 °C. Afterwards, the products were cooled to room temperature along with the furnace. Ultimately, the white samples were crushed into powders for further measurements.

2.2 Characterization

X-ray diffraction (XRD) patterns of the as-prepared samples were recorded in a Bruker D8 Advance diffractometer ($20° \leq 2\theta \leq 70°$, Cu Kα radiation, λ = 1.5405 Å) operating at 40 kV and 40 mA, with the scanning range 2θ = 5–90° and the scanning rate of 5° min^{-1}. Structural refinement was conducted using the GASA software. The morphology and chemical elements analysis of the representative sample were obtained by using the field emission scanning electron microscope (FE-SEM) with an energy-dispersive system (Zeiss Gemini SEM 300). The UCL spectra were collected on an OmniFluo960 SP-RT spectrometer coupled with a 5 W 980 nm pulse laser source at room temperature. Additionally, the temperature-dependent luminescence behavior measurement was implemented with the aid of a temperature control system RTL450 associated with the spectrometer. All the measurements were conducted at room temperature except the temperature-dependent UCL spectra.

3. Results and discussion

The XRD patterns, with corresponding crystal planes of representative $NaLaTi_2O_6$ and $NaLa_{0.99-x}Ti_2O_6$:xYb^{3+},$0.01Tm^{3+}$ (x = 0–0.30) phosphors, were collected and are exhibited in Fig. 1a. It is clearly seen that all the diffraction positions are well indexed to the bars calculated from the standard card of $NaLaTi_2O_6$ compound (ICSD 51029).[24] No other impurities

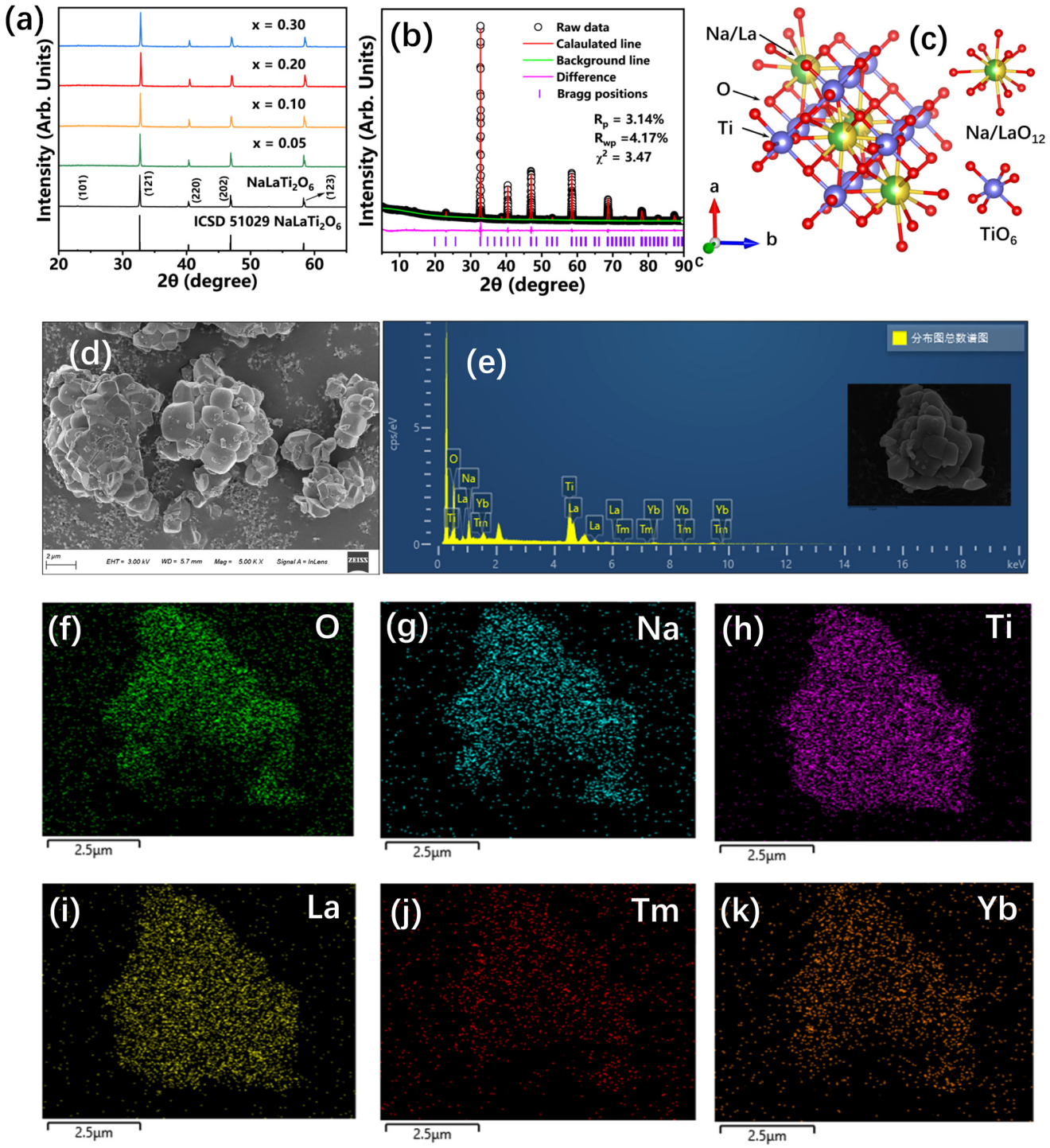

Fig. 1 (a) XRD patterns of $NaLaTi_2O_6$ host and $NaLa_{0.99-x}Ti_2O_6$:xYb^{3+},$0.01Tm^{3+}$ (x = 0.05, 0.10, 0.20, and 0.30), as well as the standard diffraction reflections calculated from the $NaLaTi_2O_6$ compound (ICSD 51029). (b) XRD Rietveld refinement profiles for $NaLa_{0.89}Ti_2O_6$:$0.10Yb^{3+}$,$0.01Tm^{3+}$. (c) Crystal structure of the $NaLaTi_2O_6$ compound and the coordination condition of Na/La and Ti atoms. (d) FE-SEM graph, (e) EDS spectrum and (f)–(k) elemental mapping of the $NaLa_{0.89}Ti_2O_6$:$0.10Yb^{3+}$,$0.01Tm^{3+}$ microparticles.

diffraction reflections can be observed, indicating that the target materials with pure phase were successfully synthesized and the incorporation of Yb^{3+} or Tm^{3+} did not arouse any structural changes in the lattice. To further provide a demonstration of pure phase samples, the XRD Rietveld refinement for the representative $NaLa_{0.89}Ti_2O_6$:$0.10Yb^{3+}$,$0.01Tm^{3+}$ was implemented, in which the data of $NaLaTi_2O_6$ compound (ICSD 51029) was taken as the original model. The refined

Table 1 Rietveld XRD refinement data for $NaLa_{0.89}Ti_2O_6$:0.10Yb^{3+}, 0.01Tm^{3+}

Material	Standard $NaLaTi_2O_6$	$NaLa_{0.89}Ti_2O_6$:0.10Yb^{3+}, 0.01Tm^{3+}
Crystal system	Orthorhombic	Orthorhombic
Space group	*Pnma*(62)	*Pnma*(62)
a (Å)	5.474	5.472
b (Å)	7.754	7.721
c (Å)	5.479	5.468
Volume (Å^3)	232.52	231.005
$\alpha = \beta = \gamma$ (°)	90	90
Z	1	1
χ^2	—	3.47
R_p (%)	—	3.14
R_{wp} (%)	—	4.17

results are displayed in Fig. 1b and Table 1. It was found that the reliability factors of both R_p = 3.14% and R_{wp} = 4.17% were much lower than 10%, in addition to χ^2 = 3.47, implying the high reliability of refinement results, and further validating the phase purity of as-prepared samples. The unit cell of the $NaLaTi_2O_6$ compound is displayed in Fig. 1c,[24] which crystallizes in a $CaTiO_3$-type perovskites double-cell cubic structure (orthorhombic) system with a space group *Pnma*(62). Apparently, Na^+ and La^{3+} cations situate at the identical lattice position Wyckoff 4*c* with equal occupancy, both of which are coordinated with twelve oxygen atoms to establish Na/LaO_{12} polyhedra. Moreover, Ti^{4+} cations located at the Wyckoff 4*b* lattice site are coordinated with six oxygen atoms to form TiO_6 octahedra. These two types of polyhedra in contiguous layers are connected by the bridge of oxygen atoms to build the skeleton of the crystal structure. The radii of Na^+ (coordination number, CN = 12), La^{3+} (CN = 12), Yb^{3+} (CN = 12), and Tm^{3+} (CN = 12) ions are 1.39 Å, 1.36 Å, 1.189 Å and 1.196 Å, respectively. The radii of Yb^{3+} and Tm^{3+} ions with the same CN and charges are close to that of La^{3+} ions, whose percentage differences are calculated to be about 12.6% and 12.1%, respectively, which are within 30%.[25] Accordingly, Yb^{3+} and Tm^{3+} ions are apt to substitute Na^+/La^{3+} sites within the crystal structure. By observing the lattice parameters in Table 1 between the standard $NaLaTi_2O_6$ compound and refined $NaLa_{0.89}Ti_2O_6$:0.10Yb^{3+},0.01Tm^{3+} materials, we can find that all the cell parameters of *a*, *b*, *c* and *V* in $NaLa_{0.89}Ti_2O_6$:0.10Yb^{3+},0.01Tm^{3+} are smaller than those in standard $NaLaTi_2O_6$, indicating the successful incorporation of Yb^{3+} and Tm^{3+} into the $NaLaTi_2O_6$ compound as the ionic radii of Yb^{3+} and Tm^{3+} are smaller than that of La^{3+}.

The morphology and elemental analysis of the representative $NaLa_{0.89}Ti_2O_6$:0.10Yb^{3+},0.01Tm^{3+} phosphor was investigated by FE-SEM measurement and the collected images are shown in Fig. 1d. It is observed that the size of the particles with irregular shapes is about 2–5 μm, and some particles agglomerate together to form the aggregates, which is attributed to the high-temperature calcination treatment during the process of samples synthesis. Na, La, Ti, O, Yb and Tm elements were detected by EDX analysis in Fig. 1e, which are identical to the chemical composition of $NaLaTi_2O_6$:Yb^{3+}, Tm^{3+}, giving the verification that the target products are properly synthesized and the rare earth elements of Yb and Tm are successfully introduced into the $NaLaTi_2O_6$ host. In order to obtain the elemental distribution state, the representative elemental mapping of a $NaLaTi_2O_6$:Yb^{3+},Tm^{3+} aggregation was collected and exhibited in Fig. 1f–k. The images show that all the detected elements are dispersed homogenously in the phosphors.

UCL spectra of $NaLa_{0.99-x}Ti_2O_6$:*x*Yb^{3+},0.01Tm^{3+} (x = 0, 0.05, 0.10, 0.20, and 0.30) phosphors with different Yb^{3+} concentrations were obtained upon a 980 nm laser excitation at room temperature. As exhibited in Fig. 2a, the Tm^{3+} singly doped $NaLaTi_2O_6$ shows a weak emission, which is due to the Tm^{3+} spin-forbidden transition and its feeble absorption cross-section. With the introduction of sensitizer Yb^{3+}, all the emission bands around 474 nm ($^1G_4 \rightarrow {}^3H_6$), 650 nm ($^1G_4 \rightarrow {}^3F_4$), 696 nm ($^3F_{2,3} \rightarrow {}^3H_6$) and 800 nm ($^3H_4 \rightarrow {}^3H_6$) from Tm^{3+} are extremely enhanced. We can also find that the NIR emission around 800 nm is more intense than blue (474 nm) and red emissions (650 nm and 696 nm), which may give more FIR options in the biological window. Moreover, with increasing *x*, the Yb^{3+} concentration in $NaLa_{0.99-x}Ti_2O_6$:*x*Yb^{3+},0.01Tm^{3+} system, no obvious Stark splitting peaks were found in blue emission bands, indicating that $^1G_{4(1)}$ and $^1G_{4(2)}$ are insignificantly impacted by the crystal field effect in this host, which is a bit different from other systems.[26,27] However, the Yb^{3+} can affect the electron population of light-emitting energy levels through energy transfer between ions. In current samples, the emission intensities of bands associated with $^1G_4$ and $^3H_4$ energy levels first increase to the maximal value and then drop with further Yb^{3+} concentration, while the optimal Yb^{3+} concentrations for these two energy levels are x = 0.20 and 0.10, respectively, as exhibited in Fig. 2b, which results in the first increase and subsequent decrease of emission intensity ratio value of $^1G_4/{}^3H_4$ transition in Fig. 2c.

It is extensively accepted that UCL is an anti-Stokes luminescence process, where two or more low-energy photons are continuously absorbed, subsequently, one high-energy photon emission is generated in swift succession. To determine the UCL mechanism of $NaLaTi_2O_6$:Yb^{3+},Tm^{3+} samples, the laser pump-power dependent UCL measurement was performed and the related UCL spectra are displayed in Fig. 2d. It manifests that the profiles of each spectrum are identical to each other with increasing laser power density. However, the integral emission intensity of each band goes up monotonically with ascending the power density gradually, as seen in Fig. 2e. The relationship between emission intensity (I) and pump power intensity (P) can be clarified by the following expression:[28]

$$I \propto P^n \quad (1)$$

where n denotes the amount of NIR photons absorbed for each UCL. After converting the above formula into $\log(I) \propto n\log(P)$, the linear fittings for different transitions were performed for the raw points and the slope in Fig. 2f equals to n value by the

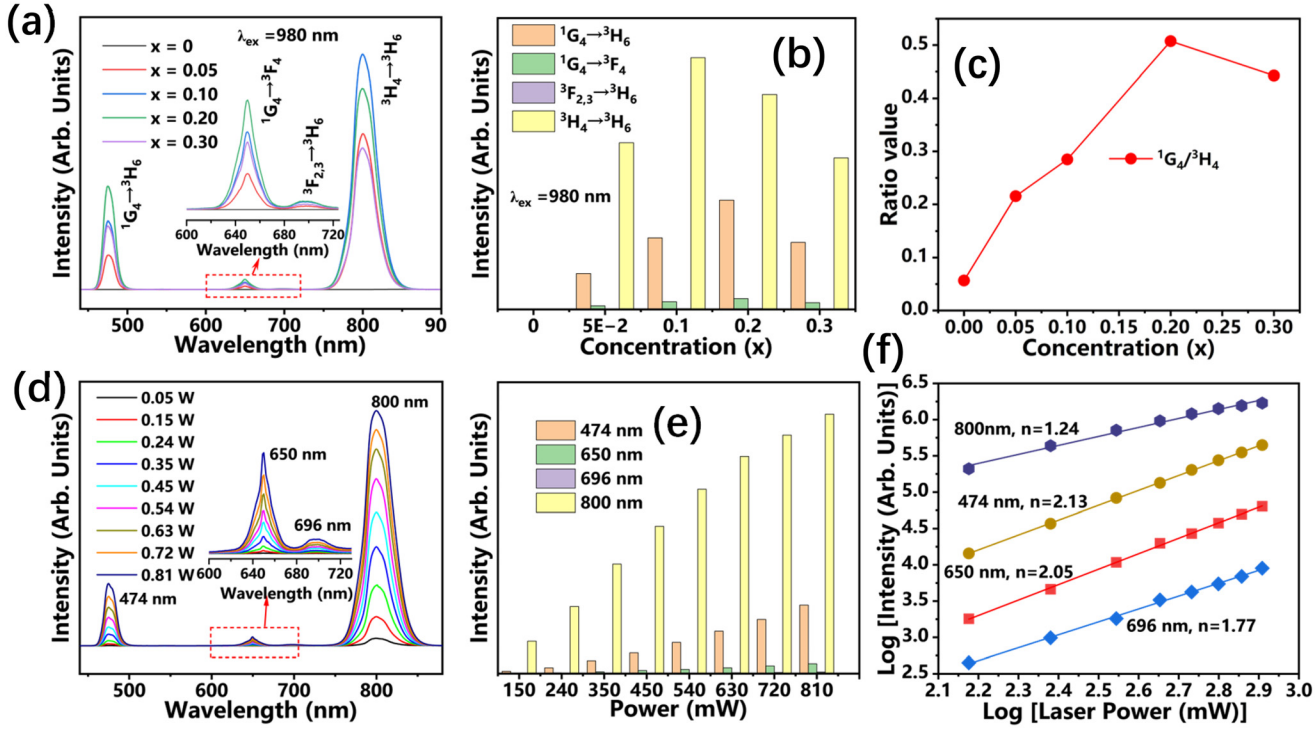

Fig. 2 (a) UCL spectra (λ_{ex} = 980 nm, laser power 0.45 W) of $NaLa_{0.99-x}Ti_2O_6$:$x$$Yb^{3+}$,0.01$Tm^{3+}$ (x = 0, 0.05, 0.10, 0.20, and 0.30) with different Yb^{3+} concentrations, and the labelled region is the enlarged spectral profile in the 600–720 nm range. (b) The corresponding emission intensities of $^1G_4 \rightarrow {}^3H_6$, $^1G_4 \rightarrow {}^3F_4$, $^3F_{2,3} \rightarrow {}^3H_6$ and $^3H_4 \rightarrow {}^3H_6$ transitions as a function of Yb^{3+} concentration. (c) The ratio variation of $^1G_4/{}^3H_4$ transition intensity as a function of Yb^{3+} concentration. (d) Laser power-dependent UCL spectra (λ_{ex} = 980 nm) for the $NaLa_{0.89}Ti_2O_6$:0.10Yb^{3+},0.01Tm^{3+} phosphor. (e) The dependence of emission intensities of 474 nm ($^1G_4 \rightarrow {}^3H_6$), 650 nm ($^1G_4 \rightarrow {}^3F_4$), 696 nm ($^3F_{2,3} \rightarrow {}^3H_6$) and 800 nm ($^3H_4 \rightarrow {}^3H_6$) on laser power. (f) Plot and linear fitting of log P *versus* log I; the slope of fitting lines gives the number of photons involved in the up-conversion process of different emission bands.

linear fitting for the disposed data. The corresponding slopes were determined to be 2.13 for 474 nm ($^1G_4 \rightarrow {}^3H_6$), 2.05 for 650 nm ($^1G_4 \rightarrow {}^3F_4$), 1.77 for 696 nm ($^3F_{2,3} \rightarrow {}^3H_6$) and 1.24 for 800 nm ($^3H_4 \rightarrow {}^3H_6$), implying that three photons participate in the former two UCL process and two photons are concerned in the latter two emission process. The slopes are much less than standard 3 and 2 for three and two photons and may be ascribed to the saturation effect that reduces the power dependence of emissions.[29]

According to the analysis above, the energy transfer mechanism between Yb^{3+} and Tm^{3+} ions, as well as the probable UCL processes, are proposed in Fig. 3. As Tm^{3+} has weak absorption in the NIR region, herein, the Yb^{3+} ions acting as the sensitizers with a large cross-section absorption around 980 nm were first excited from $^2F_{7/2}$ to $^2F_{5/2}$ energy levels upon 980 nm laser pumping, and then the energy absorbed was transferred to the $^3H_5$ level of Tm^{3+} (labelled as ET1 process). Afterward, the electrons at the $^3H_5$ energy level non-radiatively relax to the $^3F_4$ energy level and can be pumped to the $^3F_{2,3}$ energy level by absorbing another photon (labelled as ET2 process). Then, the 696 nm emission band is produced from the $^3F_{2,3} \rightarrow {}^3H_6$ transition directly. Simultaneously, the 800 nm emission band is generated from the $^3H_4 \rightarrow {}^3H_6$ transition when electrons at the $^3F_{2,3}$ energy level non-radiatively relax to the $^3H_4$ energy level.

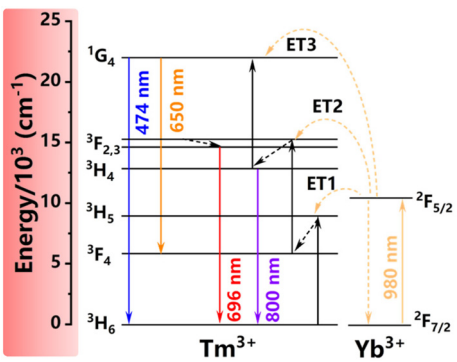

Fig. 3 Proposed diagram of energy levels and up-conversion luminescence mechanism in $NaLaTi_2O_6$:Yb^{3+},Tm^{3+} phosphors upon 980 nm excitation.

Besides, the electrons at the $^3H_4$ energy level can also be populated to the $^1G_4$ energy level by absorbing another photon (labelled as ET3) and 474 nm and 650 nm emissions are directly obtained by experiencing the $^1G_4 \rightarrow {}^3H_6$ and $^1G_4 \rightarrow {}^3F_4$ transitions, respectively.[30,31]

To investigate the potential application of the as-prepared samples in optical thermometry, temperature-dependent UCL

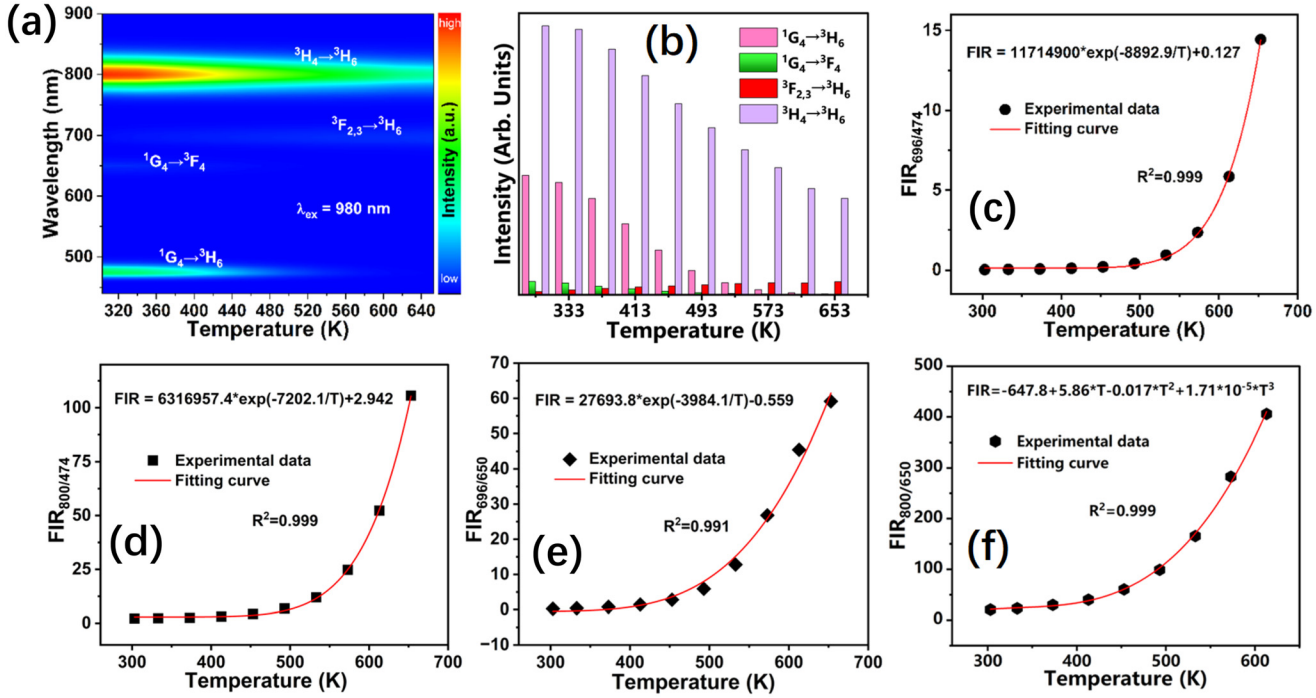

Fig. 4 (a) The contour map of the thermal evolution UCL spectrum in the temperature range of 303 K–653 K for the $NaLa_{0.89}Ti_2O_6$:0.10Yb^{3+},0.01Tm^{3+} phosphor upon 980 nm excitation with a laser power of 0.45 W. (b) The corresponding emission intensities of $^1G_4 \rightarrow {}^3H_6$, $^1G_4 \rightarrow {}^3F_4$, $^3F_{2,3} \rightarrow {}^3H_6$ and $^3H_4 \rightarrow {}^3H_6$ transitions as a function of temperature. Temperature dependence of experimentally measured UCL intensity ratio of I_{696}/I_{474} (c), I_{800}/I_{474} (d), I_{696}/I_{650} (e), and I_{800}/I_{650} (f) and corresponding fitting curves from eqn (2) or (5).

behavior of typical $NaLa_{0.89}Ti_2O_6$:0.10Yb^{3+},0.01Tm^{3+} sample upon 980 nm excitation was assessed and the contour map of thermal evolution UCL spectrum in the temperature range of 303 K–653 K is presented in Fig. 4a. It is found that the emission position for UCL peak does not change with the increase of temperature. However, the emission intensities of 474 nm ($^1G_4 \rightarrow {}^3H_6$), 650 nm ($^1G_4 \rightarrow {}^3F_4$), and 800 nm ($^3H_4 \rightarrow {}^3H_6$) bands drop monotonously at different extents with increasing temperature, which is due to the general thermal quenching effect. It is highlighted that the peaks at 474 and 650 nm greatly decrease to about one-139th and one-52th, respectively, more dramatically than that of the three 10th for 800 nm. It is worth noting that the 696 nm ($^3F_{2,3} \rightarrow {}^3H_6$) emission conquers the thermal quenching effect and is gradually enhanced more than ten-fold when the temperature increases from 303 K to 653 K, which would be owing to the phonon-assisted energy transfer from Yb^{3+} to Tm^{3+}.[32] Energy transfer from Yb^{3+} to Tm^{3+} would facilitate the population of the $^3F_{2,3}$ excited levels, subsequently leading to intensified emission with increasing temperature. These high-contrast temperature-dependent UCL characteristics can be expected to gain a highly sensitive FIR thermometry. For explicit comprehension, four types of FIR models, involving the $^3F_{2,3} \rightarrow {}^3H_6/{}^1G_4 \rightarrow {}^3H_6$ (I_{696}/I_{474}), $^3H_4 \rightarrow {}^3H_6/{}^1G_4 \rightarrow {}^3H_6$ (I_{800}/I_{474}), $^3F_{2,3} \rightarrow {}^3H_6/{}^1G_4 \rightarrow {}^3F_4$ (I_{696}/I_{650}) and $^3H_4 \rightarrow {}^3H_6/{}^1G_4 \rightarrow {}^3F_4$ (I_{800}/I_{650}) transitions, were employed for temperature-monitored signals. With increasing temperature from 303 K to 653 K, the FIR values for these four models go up gradually. As there is no TCEL transition concerned in them, it is illustrated that the former three FIR data can be well fitted with the equation below:[33,34]

$$\mathrm{FIR} = A\exp\left(-\frac{B}{T}\right) + C \tag{2}$$

where A, B, and C are fitting constants, and T is the absolute temperature. As depicted in Fig. 4c–e, the fitted A, B, and C values are 11 714 900, 8892.9 and 0.127 for $FIR_{696/474}$, 6 326 957.4, 7202.1 and 2.942 for $FIR_{800/474}$, 27 693.8, 3984.1 and −0.559 for $FIR_{696/650}$. In addition, to evaluate the performance of the devised thermometers, absolute sensitivity (S_a) and relative sensitivity (S_r) are calculated using the following equations:

$$S_a = \left|\frac{\mathrm{dFIR}}{\mathrm{d}T}\right| = \frac{B}{T^2} \times A\exp\left(-\frac{B}{T}\right) \tag{3}$$

$$S_r = \frac{1}{\mathrm{FIR}}\left|\frac{\mathrm{dFIR}}{\mathrm{d}T}\right| = \frac{B}{T^2} \times A\exp\left(-\frac{B}{T}\right) \times \frac{1}{\mathrm{FIR}} \tag{4}$$

According to the equations above, the S_a and S_r values are calculated and presented in Fig. 5a–c. It is observed that the S_a and S_r values for $FIR_{696/474}$ present different tendencies as temperature increases, with the maximal values of 0.298 K^{-1}@653 K and 36.2% K^{-1}@303 K, respectively. Similarly, the maximal S_a and S_r values are determined to be 1.73 K^{-1}@653 K and 2.40% K^{-1}@303 K for $FIR_{800/474}$ and 0.557 K^{-1}@653 K and 14.1% K^{-1}@303 K for $FIR_{696/650}$, respectively. Fascinatingly, these obtained S_a and S_r values are much

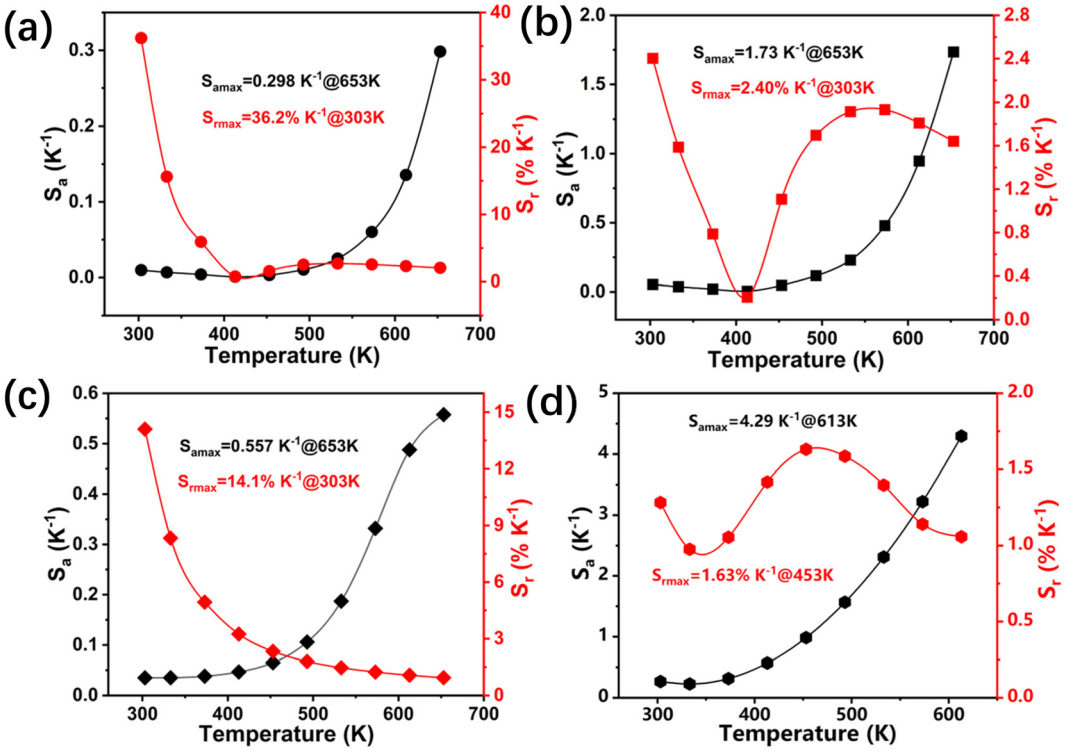

Fig. 5 Calculated S_a and S_r values of the $NaLa_{0.89}Ti_2O_6$:0.10Yb^{3+},0.01Tm^{3+} phosphor based on the FIR of I_{696}/I_{474} (a), I_{800}/I_{474} (b), I_{696}/I_{650} (c), and I_{800}/I_{650} (d).

Table 2 The comparison of maximal absolute ($S_{a\text{-}max}$) and relative ($S_{a\text{-}max}$) sensitivities of Ln^{3+} or transition metal ion activated luminescent thermometers

Materials	Temperature range (K)	$S_{a\text{-}max}$ (K^{-1})	$S_{r\text{-}max}$ (K^{-1}%)	Ref.
$NaY(WO_4)_2$:Yb,Er	295–503	0.008	1.2	37
$CaGdMgSbO_6$:Mn^{4+},Sm^{3+}	298–573	0.0138	1.54	38
Ca_2GdSbO_6:Mn^{4+},Sm^{3+}	303–503	0.26	1.55	39
ZrO_2:Ti,Eu	303–413	0.41	3.84	40
$SrTiO_3$:Mn^{4+},Er^{3+}	100–470	—	5.19	41
$Sr_3Y(PO_4)_3$:Tm^{3+},Yb^{3+}	293–573	0.0127	1.52	42
Bi_2SiO_5:Tm^{3+},Yb^{3+}@SiO_2	280–400	0.0168	1.95	43
$BaTiO_3$:Er^{3+}/Yb^{3+}/Zn^{2+}	120–505	0.095	1.46	44
$CaIn_2O_4$:Yb^{3+},Tm^{3+},Er^{3+}	313–513	0.123	1.484	35
Al_2O_3:Sm^{2+}	298–648	—	4.8	45
SrB_4O_7:Sm^{2+}	298–723	—	3.36	46
$GdAlO_3$:Eu^{3+}	293–793	—	2.96	47
$Li_{1.8}Na_{0.2}TiO_3$:Mn^{4+}	10–350	—	2.27	48
$NaLaTi_2O_6$:Yb^{3+},Tm^{3+} ($FIR_{696/474}$)	303–653	0.298	36.2	This work
$NaLaTi_2O_6$:Yb^{3+},Tm^{3+} ($FIR_{800/474}$)	303–653	1.73	2.40	This work
$NaLaTi_2O_6$:Yb^{3+},Tm^{3+} ($FIR_{696/650}$)	303–653	0.557	14.1	This work
$NaLaTi_2O_6$:Yb^{3+},Tm^{3+} ($FIR_{800/650}$)	303–613	4.29	1.63	This work

higher than those of other reported optical thermometers in an order of magnitude, at least based on TCEL or NTCEL transitions, as listed in Table 2. For $FIR_{800/650}$, it is found that a polynomial equation rather than the eqn (2) is more suitable for fitting FIR values of transitions $^3H_4 \rightarrow {}^3H_6/{}^1G_4 \rightarrow {}^3F_4$ (I_{800}/I_{650}) in Fig. 4f,[35,36] which is depicted as follows:

$$\mathrm{FIR} = A_0 + A_1 \times T + A_2 \times T^2 + A_3 \times T^3 \quad (5)$$

where A_0, A_1, A_2 and A_3 are fitting constants of the polynomial. The corresponding absolute and relative sensitivity can be calculated by the following equation:

$$S_a = A_1 + 2A_2 \times T + 3A_3 \times T^2 \quad (6)$$

$$S_r = \frac{1}{\mathrm{FIR}}(A_1 + 2A_2 \times T + 3A_3 \times T^2) \quad (7)$$

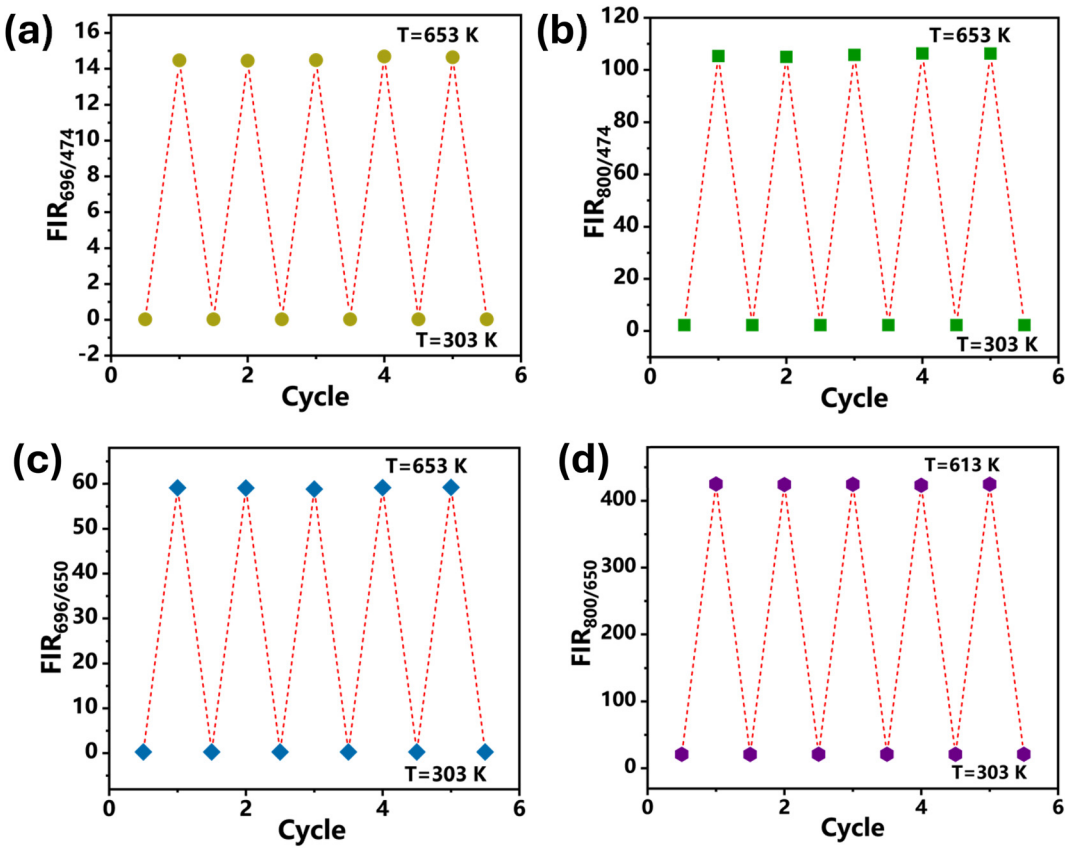

Fig. 6 Repeatability of different FIRs measured over 5 heating and cooling cycling measurements for I_{696}/I_{474} (a), I_{800}/I_{474} (b), I_{696}/I_{650} (c), and I_{800}/I_{650} (d).

Using eqn (6) and (7), the calculated S_a and S_r values are displayed in Fig. 5d. The maximal value of S_a reaches 4.29 K^{-1}@653 K and the maximal S_r is 1.63% K^{-1}@453 K, which is also much higher than that from the reported works listed in Table 2.

The repeatability (R) of the thermometer is an important parameter to assess the stability of the thermometer, which is reflected by cycling over heating–cooling processes, as displayed in Fig. 6a–d. The expression of R can be described as follows:[49,50]

$$R = 1 - \frac{\mathrm{Max}|\Delta_m - \Delta_i|}{\Delta_m} \quad (8)$$

where Δ_m and Δ_i are the mean value of FIR (303 and 653 K or 613 K) and FIR value in continuous 5 measurement cycles, respectively. Fig. 6a–d presents the cycling measurement of different FIR values of the $NaLaTi_2O_6$:0.10Yb^{3+},0.01Tm^{3+} phosphor. The repeatability of $NaLa_{0.89}Ti_2O_6$:0.10Yb^{3+},0.01Tm^{3+} sample was calculated to be more than 0.990, which indicates the wonderful reversibility of the expected FIR thermometry.

In addition, the temperature uncertainty (δT) is also one of the most vital parameters to evaluate the performance of a FIR optical thermometer and is denoted as follows:[51,52]

$$\delta T = \frac{1}{S_r}\frac{\delta \mathrm{FIR}}{\mathrm{FIR}} \quad (9)$$

where δFIR/FIR is the relative error of the experimental equipment when it is used for the measurement of thermometric parameters (~0.5%).[53] Accordingly, the minimal δT is estimated to be ~0.0138 K at 303 K, implying high measuring accuracy. The above results indicate that the as-prepared samples have great temperature sensing performance, giving them giant potential in the temperature sensing application.

4. Conclusions

To sum up, a series of $NaLaTi_2O_6$:Yb^{3+},Tm^{3+} phosphors were successfully synthesized using a high-temperature solid-state reaction approach. The as-prepared samples are demonstrated to be the pure $NaLaTi_2O_6$ phase from XRD measurements. UCL spectra exhibit moderately blue and stronger NIR emissions upon the 980 nm laser excitation, as well as the two weak red emissions. The laser pump-power-dependent UCL spectra implied a two-photon or three-photon absorption mechanism in the UCL process. The temperature-dependent UCPL spectra were recorded, which display the emission bands of Tm^{3+} $^1G_4 \rightarrow {}^3H_6$, $^1G_4 \rightarrow {}^3F_4$, and $^3H_4 \rightarrow {}^3H_6$ transitions, which weaken with increasing temperature at distinct extents due to the general thermal quenching effect. Surprisingly, the thermal enhancement of Tm^{3+} $^3F_{2,3} \rightarrow {}^3H_6$ transition (red emission)

takes place, which is likely derived from the phonon-assisted energy transfer effect. By virtue of tunable luminescence responses to temperature, we systematically investigated the FIR-based temperature sensing properties of $NaLa_{0.89}Ti_2O_6$:0.10Yb^{3+},0.01Tm^{3+} phosphor. Depending on the high contrast thermal dependent performances for different transitions, the devised luminescence thermometry acquired fascinating S_a and S_r values of 4.29 K^{-1}@613 K and 36.2% K^{-1}@303 K, respectively, which are an order of magnitude higher than the reported results, and present high repeatability (99.0%). The unprecedented ratiometric temperature sensing performance strongly enables the as-prepared $NaLaTi_2O_6$:Yb^{3+},Tm^{3+} phosphors to have promising applications as a temperature sensor in the optical temperature sensing field. Simultaneously, this work will encourage us to devise highly stable and sensitive temperature sensors by taking advantage of the Tm^{3+}-activated luminescence phosphors.

Data availability

We all declare that all relevant data are within the paper and no additional data are available.

Conflicts of interest

There are no conflicts to declare.

Acknowledgements

This research was supported by the Science Foundation of China University of Petroleum, Beijing (No. 2462022QNXZ003 and SKLHOP2023115810), the Fundamental Research Funds for the Central Universities (No. 2023MS025), and the Young Scholar Fostering Project at NCEPU (No. XM2312301).

References

1 Y. Cui, R. Song, J. Yu, M. Liu, Z. Wang, C. Wu, Y. Yang, Z. Wang, B. Chen and G. Qian, Dual-emitting MOF∩Dye composite for ratiometric temperature sensing, *Adv. Mater.*, 2015, **27**, 1420–1425.

2 Z. Lei, H. Dong, L. Sun, B. Teng, Y. Zou and D. Zhong, Eulytite-type $Ba_3Yb(PO_4)_3$:Tm/Er/Ho as a high sensitivity optical thermometer over a broad temperature range, *J. Mater. Chem. C*, 2024, **12**, 628–638.

3 L. Sun, $NaBiF_4$-based hollow upconversion nanoparticles for temperature sensing, *Light: Sci. Appl.*, 2022, **11**, 257.

4 S. Sadat, A. Tan, Y. J. Chua and P. Reddy, Nanoscale thermometry using point contact thermocouples, *Nano Lett.*, 2010, **10**, 2613–2617.

5 Y. Zi, Z. Yang, Z. Xu, X. Bai, A. Ullah, I. Khan, A. A. Haider, J. Qiu, Z. Song, Y. Wang and Y. Cun, A novel upconversion luminescence temperature sensing material: Negative thermal expansion $Y_2Mo_3O_{12}$:Yb^{3+},Er^{3+} and positive thermal expansion $Y_2Ti_2O_7$:Yb^{3+},Er^{3+} mixed phosphor, *J. Alloys Compd.*, 2021, **880**, 160156.

6 M. D. Dramićanin, Trends in luminescence thermometry, *J. Appl. Phys.*, 2020, **128**, 040902.

7 Y. C. Jiang, Y. Tong, S. Y. Z. Chen, W. N. Zhang, F. F. Hu, R. F. Wei and H. Guo, A three-mode self-referenced optical thermometry based on up-conversion luminescence of Ca_2MgWO_6:Er^{3+},Yb^{3+} phosphors, *Chem. Eng. J.*, 2021, **413**, 127470.

8 Y. Pan, X. Xie, Q. Huang, C. Gao, Y. Wang, L. Wang, B. Yang, H. Su, L. Huang and W. Huang, Inherently Eu^{2+}/Eu^{3+} codoped Sc_2O_3 nanoparticles as high performance nanothermometers, *Adv. Mater.*, 2018, **30**, 1705256.

9 Q. Xiao, B. Liu, C. Song, S. Wu, L. Yang, J. Guo, X. Wu, N. Zhou, X. Yin and X. Luo, 808 nm excited multi-color upconversion luminescence and optical temperature sensing through Yb^{3+}-mediated energy transfer in Nd^{3+}-sensitized system, *Ceram. Int.*, 2024, **50**, 6154–6164.

10 A. Pandey, V. K. Rai, V. Kumar, V. Kumar and H. C. Swart, Upconversion based temperature sensing ability of Er^{3+}–Yb^{3+} codoped $SrWO_4$: an optical heating phosphor, *Sens. Actuators, B*, 2015, **209**, 352–358.

11 K. Zheng, G. He, W. Song, X. Bi and W. Qin, A strategy for enhancing the sensitivity of optical thermometers in β-$NaLuF_4$:Yb^{3+}/Er^{3+} nanocrystals, *J. Mater. Chem. C*, 2015, **3**, 11589–11594.

12 D. Zhang, Y. Luo, J. Chen, L. Li and H. Guo, A dual-mode optical thermometer based on dual-excitation Bi^{3+}, Sm^{3+} co-doped Y_4GeO_8 phosphors, *J. Rare Earths*, 2024, **42**, 1437–1446.

13 J. Y. Chen, J. Q. Chen, L. J. Li, W. N. Zhang, L. P. Chen and H. Guo, A four-mode high-sensitive optical thermometer based on $Ca_3LiZnV_3O_{12}$:Sm^{3+} phosphors, *Mater. Today Chem.*, 2023, **29**, 101409.

14 H. Du, Y. Liang, X. Liu, Y. Deng, J. Yang, J. Yang and S. Hu, Upconversion luminescence and temperature sensing properties of $Yb_2(MoO_4)_3$:Ln^{3+} (Ln = Ho, Tm, Er) phosphors based on energy transfer, *CrystEngComm*, 2023, **25**, 5452–5460.

15 J. Feng, Z. Fu, Z. Wang and H. Xu, Design strategies for three highly sensitive multimodal optical thermometers based on diverse luminescence thermal-response in $BaLu_2Si_3O_{10}$:Ln^{3+},Yb^{3+} phosphors (Ln^{3+} = Er^{3+}, Ho^{3+}, Nd^{3+}), *Ceram. Int.*, 2023, **49**, 29036–29047.

16 O. A. Lipina, L. L. Surat, A. Yu. Chufarov, I. V. Baklanova, A. N. Enyashin, M. A. Melkozerova, A. P. Tyutyunnik and V. G. Zubkov, Structural, electronic and optical properties of $BaRE_6(Ge_2O_7)_2(Ge_3O_{10})$ (RE = Tm, Yb, Lu) compounds and $BaYb_6(Ge_2O_7)_2(Ge_3O_{10})$:$Tm^{3+}$ and $BaLu_6(Ge_2O_7)_2(Ge_3O_{10})$:$Yb^{3+}$, Tm^{3+} phosphors: potential applications in temperature sensing, *Dalton Trans.*, 2023, **52**, 7482–7494.

17 W. You, X. Zhang, R. Yu, C. Chen, M. Li, G. Pan and Y. Mao, Highly efficient upconversion luminescence in narrow-bandgap $Y_2Mo_4O_{15}$, *Opt. Lett.*, 2024, **49**, 1824–1827.

18 Q. Xiao, X. Dong, X. Yin, H. Wang, H. Zhong, K. Liu, B. Dong and X. Luo, Promising Yb^{3+}-sensitized $La_2Mo_2O_9$ phosphors for multi-color up-conversion luminescence and optical temperature sensing, *J. Alloys Compd.*, 2022, **895**, 162686.

19 X. Zhang, H. Zheng, J. Hu, F. Lu, X. Peng, R. Wei, F. Hu and H. Guo, Enhanced up-conversion luminescence and temperature sensing property of $Ba_{3-x}Sr_xLu_4O_9$:Tm^{3+}/Yb^{3+} phosphors, *Ceram. Int.*, 2021, **47**, 32290–32296.

20 A. Zhou, F. Song, F. Song, M. Feng, K. Adnan, D. Ju and X. Wang, Optical thermometry using fluorescence intensities multi-ratios in $NaGdTiO_4$:Yb^{3+}/Tm^{3+} phosphors, *Opt. Mater.*, 2018, **78**, 438–444.

21 Z. Sun, G. Liu, Z. Fu, X. Zhang, Z. Wu and Y. Wei, High sensitivity thermometry and optical heating Bi-function of Yb^{3+}/Tm^{3+} Co-doped $BaGd_2ZnO_5$ phosphors, *Curr. Appl. Phys.*, 2017, **17**, 255–261.

22 Y. Fu, X. Wang, S. Liu, H. Wang, Y. Tian, M. Xing, Q. Pang, F. Xin and X. Luo, Multicolor upconversion emission and highly optical temperature sensing based on lanthanide-doped double perovskite Sr_2LaNbO_6 phosphors, *Ceram. Int.*, 2023, **49**, 9574–9583.

23 L. Cao, Z. Wang, P. Cai, X. Hu, B. Zhang, X. Chu and S. Li, Up-conversion luminescence properties of $LuVO_4$:Yb^{3+}/Tm^{3+}/Er^{3+} submicron materials for high sensitivity temperature probing, *J. Mater. Sci.: Mater. Electron.*, 2021, **32**, 28088–28097.

24 Z. Zhang, H. Zhang, M. Xu, X. Zong, F. Han, X. Ma, X. Li and D. Wang, Photoluminescence properties of a novel red emitting $NaLaTi_2O_6$:Eu^{3+} phosphor, *J. Mater. Sci.: Mater. Electron.*, 2016, **27**, 724–729.

25 S. Wei, Z. Lyu, D. Sun, P. Luo, Z. Lu, L. Zhou, M. He, S. Shen and H. You, Energy transfer and tunable emission in $BaSrGd_4O_8$:Bi^{3+},Eu^{3+} phosphors for warm WLED, *Dalton Trans.*, 2023, **52**, 17966–17973.

26 Y. Liang, D. Wang, H. Wu, S. Hu and J. Yang, Luminescence and temperature sensing properties of KLu$(MoO_4)_2$:Ln^{3+} phosphors, *Opt. Mater.*, 2022, **133**, 112879.

27 M. Xing, T. Pang, L. Yan, L. Kang, X. Wu, H. Wang, Y. Fu, X. Luo and Y. Tian, Integration of high-thermal-responsive color change and invisible emission intensity ratio in $Gd_2Mo_4O_{15}$ lattice with the desired structure, *Mater. Today Chem.*, 2023, **27**, 101304.

28 X. F. Wang, Q. Liu, P. Q. Cai, J. Wang, L. Qin, T. Q. Vu and H. J. Seo, Excitation powder dependent optical temperature behavior of Er^{3+} doped transparent $Sr_{0.69}La_{0.31}F_{2.31}$ glass ceramics, *Opt. Express*, 2016, **24**, 17792–11804.

29 X. Huang, J. Liu, H. Pan, C. Tian, H. Zhang, X. Chen, A. Huang and Z. Xiao, Temperature-dependent upconversion luminescence and spectra characteristic of Er^{3+}/Yb^{3+} co-doped fluorotellurite glasses, *J. Lumin.*, 2019, **207**, 41–47.

30 L. Li, X. Cao, Y. Zhang and C. Guo, Synthesis and upconversion luminescence of Lu_2O_3:Yb^{3+}, Tm^{3+} nanocrystals, *Trans. Nonferrous Met. Soc. China*, 2012, **22**, 373–379.

31 Z. Li, Z. Lyu, D. Sun, S. Shen and H. You, The downshifting and upconversion photoluminescence from $NaBaSc_2(PO_4)_3$ for multicolor anti-counterfeiting, *Mater. Today Chem.*, 2022, **26**, 101116.

32 M. Dai, Y. Li, Z. Wang, A. Li, T. Sheng, H. Xu, K. Li and Z. Fu, Thermally boosted upconversion luminescence and high-performance thermometry in ScF_3:Yb^{3+}/Tm^{3+} nanorods with negative thermal expansion, *J. Lumin.*, 2024, **265**, 120219.

33 Q. Zhang, L. Li, F. Liu, S. Li, X. Wei, W. Wang, H. Chen, Y. Pan and Y. Li, Optical thermometry of Tm^{3+}/Yb^{3+} Co-doped $Ba_3Gd_2F_{12}$ up-conversion glass-ceramic with high sensitivity, *J. Solid State Chem.*, 2022, **308**, 122927.

34 Z. Li, X. Yu, T. Wang, S. Wang, L. Guo, Z. Cui, G. Yan, W. Feng, F. Zhao, J. Chen, X. Xu and J. Qiu, *J. Am. Ceram. Soc.*, 2022, **105**, 2804–2812.

35 H. Liu, Z. Zhang, J. Liu, K. Wang and Y. Zhang, Efficient upconversion and downshifting luminescence of $CaIn_2O_4$: Yb^{3+}/Tm^{3+}/RE^{3+} (RE = Er/Ho) phosphor: Temperature sensing performance in the visible and near-infrared range, *Ceram. Int.*, 2023, **49**, 30510–30521.

36 Q. Wang, M. Liao, Q. Lin, M. Xiong, Z. Mu and F. Wu, A review on fluorescence intensity ratio thermometer based on rare-earth and transition metal ions doped inorganic luminescent materials, *J. Alloys Compd.*, 2021, **850**, 156744.

37 M. Lin, L. Xie, Z. Wang, B. S. Richards, G. Gao and J. Zhong, Facile synthesis of monodisperse sub-20 nm NaY$(WO_4)_2$:Er^{3+}, Yb^{3+} upconversion nanoparticles: a new choice for nanothermometry, *J. Mater. Chem. C*, 2019, **7**, 2971–2977.

38 J. Liao, M. Wang, L. Kong, J. Chen, X. Wang, H. Yan, J. Huang and C. Tu, Dual-mode optical temperature sensing behavior of double-perovskite $CaGdMgSbO_6$: Mn^{4+}/Sm^{3+} phosphors, *J. Lumin.*, 2020, **226**, 117492.

39 G. Li, Y. Xue, Q. Mao, L. Pei, H. He, M. Liu, L. Chu and J. Zhong, Synergistic luminescent thermometer using co-doped Ca_2GdSbO_6:Mn^{4+}/(Eu^{3+} or Sm^{3+}) phosphors, *Dalton Trans.*, 2022, **51**, 4685–4694.

40 G. Pan, L. Zhang, H. Wu, X. Qu, H. Wu, Z. Hao, L. Zhang, X. Zhang and J. Zhang, On the luminescence of Ti^{4+} and Eu^{3+} in monoclinic ZrO_2: high performance optical thermometry derived from energy transfer, *J. Mater. Chem. C*, 2020, **8**, 4518–4533.

41 W. M. Piotrowski, K. Trejgis, M. Dramicanin and L. Marciniak, Strong sensitivity enhancement in lifetime-based luminescence thermometry by co-doping of $SrTiO_3$: Mn^{4+} nanocrystals with trivalent lanthanide ions, *J. Mater. Chem. C*, 2021, **9**, 10309–10316.

42 W. Liu, X. Wang, Q. Zhu, X. Li, X. Sun and J. G. Li, Upconversion luminescence and favorable temperature sensing performance of eulytite-type $Sr_3Y(PO_4)_3$:Yb^{3+}/Ln^{3+} phosphors (Ln = Ho, Er, Tm), *Sci. Technol. Adv. Mater.*, 2019, **20**, 949–963.

43 E. Casagrande, M. Back, D. Cristofori, J. Ueda, S. Tanabe, S. Palazzolo, F. Rizzolio, V. Canzonieri, E. Trave and P. Riello, Upconversion-mediated Boltzmann thermometry in double-layered Bi_2SiO_5:Yb^{3+},Tm^{3+}@SiO_2 hollow nanoparticles, *J. Mater. Chem. C*, 2020, **8**, 7828–7836.

44 M. K. Mahata, T. Koppe, T. Mondal, C. Brüsewitz, K. Kumar, V. K. Rai, H. Hofsass and U. Vetter, Incorporation of Zn^{2+} ions into $BaTiO_3$:Er^{3+}/Yb^{3+} nanophosphor: an effective way to enhance up conversion, defect luminescence and temperature sensing, *Phys. Chem. Chem. Phys.*, 2015, **17**, 20751.

45 A. Ćirić, S. Stojadinović, Z. Ristić, I. Zeković, S. Kuzman, Ž. Antić and M. D. Dramićanin, *Adv. Mater. Technol.*, 2021, **6**, 2001201.

46 Z. Cao, X. Wei, L. Zhao, Y. Chen and M. Yin, Investigation of SrB_4O_7:Sm^{2+} as a Multimode Temperature Sensor with High Sensitivity, *ACS Appl. Mater. Interfaces*, 2016, **8**, 34546–34551.

47 V. Lojpur, S. Ćulubrk, M. Medić and M. Dramicanin, Luminescence thermometry with Eu^{3+} doped $GdAlO_3$, *J. Lumin.*, 2016, **170**, 467–471.

48 M. Sekulić, Z. Ristić, B. Milićević, Ž. Antić, V. Đorđević and M. D. Dramićanin, $Li_{1.8}Na_{0.2}TiO_3$:Mn^{4+}: The highly sensitive probe for the low-temperature lifetime-based luminescence thermometry, *Opt. Commun.*, 2019, **452**, 342–346.

49 C. D. S. Brites, A. Millán and L. D. Carlos, *Handbook on the Physics and Chemistry of Rare Earths*, Elsevier, 2016, vol. 49, pp. 339–427.

50 M. Dai, Z. Fu, Z. Wang and H. Xu, Sc^{3+}-induced double optimization strategies for boosting NIR-II luminescence and improving thermometer performance in CaF_2: Nd^{3+}, Nd^{3+}/Yb^{3+}@$NaYF_4$ nanocrystals, *Chem. Eng. J.*, 2023, **452**, 139133.

51 C. Brites, S. Balabhadra and L. Carlos, Lanthanide-based thermometers: at the cutting-edge of luminescence thermometry, *Adv. Opt. Mater.*, 2019, **7**, 1801239.

52 K. Soler-Carracedo, I. R. Martin, M. Runowski, L. L. Martín, F. Lahoz, A. D. Lozano-Gorrín and F. Paz-Buclatin, Luminescent Nd^{3+}-Based Microresonators Working as Optical Vacuum Sensors, *Adv. Opt. Mater.*, 2020, **8**, 2000678.

53 J. Wang, J. Li, R. Lei, S. Zhao and S. Xu, Single band ratiometric luminescence thermometry based on Pr^{3+} doped oxides containing charge transfer states, *J. Mater. Chem. C*, 2022, **10**, 12413–12421.